JOURNAL OF CHEMICAL & ENGINEERING DATA

ARTICLE

pubs.acs.org/jced

Multiwalled Carbon Nanotubes as Adsorbents for the Kinetic and Equilibrium Study of the Removal of Alizarin Red S and Morin

M. Ghaedi,*[,†] A. Hassanzadeh,[‡] and S. Nasiri Kokhdan[‡]

[†]Chemistry Department, Yasouj University, Yasouj 75914-35, Iran

[‡]Department of Chemistry, Faculty of Science, University of Urmia, Urmia, Iran

ABSTRACT: The multiwalled carbon nanotube has been used as an efficient adsorbent for the removal of Alizarin red S (ARS) and morin from wastewater. The influence of variables including pH, temperature, concentration of the dye, amount of adsorbents and contact time, and so forth on the removal of both dyes was investigated by the batch method. Graphical correlations of various adsorption isotherm models like Langmuir, Freundlich, Tempkin, and Dubinin−Radushkevich have been carried out. The adsorption of ARS and morin has been found to be endothermic and feasible in nature. Various thermodynamic parameters, such as Gibbs free energy, entropy, and enthalpy, of the ongoing adsorption process have been calculated. The kinetic studies suggest the process following pseudosecond-order kinetics and involvement of the particle-diffusion mechanism.

1. INTRODUCTION

High amounts of contaminated dye aqueous effluents are generated by different industries. Their treatment from toxic dyes causes allergies and skin irritation in humans since most of them are mutagenic and/or carcinogenic.[1−3] Because of this, industrial effluents containing dyes need to be treated before being delivered to the environment.[4−6] The most efficient procedure for dye removal from industrial effluents is the adsorption procedure. In this process the dye species are transferred from the water effluent to a solid phase that leads to decreasing the effluent volume.

The two major groups of the anthracenes, that is, anthraquinone and naphtoquinone, contain several well-known dyes such as alizarin. Alizarin is an organic compound that is historically important as a prominent dye. It is an anthraquinone originally derived from the root of the madder plant. Alizarin red S (ARS; Figure 1; sulfone derivative of alizarin[7,8]) is a strong oxidant reagent, and in this regard it must be stored away from heat and moisture.

Morin is a major flavonoid component of the heartwood of the plant *Maclura cochinchinensis* (Lour.) Corner (family *Moraceae*). In the northeast area of Thailand, aqueous extracts of the wood of this plant are used for the dyeing of silk. The dye extract, which has morin (2′,3,4′,5,7-pentahydroxyflavone; Figure 1) as a major component, gives a fine yellow color to the silk. Unfortunately, the use of this natural dye mixture is often linked to poor fastness properties, and thus metal-based mordants are used to increase fastness (e.g., wash fastness) properties.[9]

Carbon nanotubes (CNTs) are one of the most commonly used building blocks of nanotechnology as unique and one-dimensional macromolecules that possess outstanding thermal and chemical stability.[10−15] These nanomaterials have been proven to possess great potential as adsorbents for removing many kinds of environmental pollutants.[12−16] CNTs have been considered useful in pollution prevention strategies and are known to have widespread applications as environmental adsorbents and high flux membranes[16] and are also potentially important for in situ environmental remediation due to their unique properties and high reactivity.[17−20]

Understanding the kinetics and thermodynamics of the adsorption is critical for the development of more efficient adsorbents suitable for their real environmental applications. These limited studies suggested that the adsorption of organic compounds on MWCNTs was spontaneous and mainly due to physical adsorption. CNTs with a high surface area and large micropore volume as extremely good adsorbents have been utilized for the sorption of a large number of different organic compounds from water.[21−32]

In view of the going farther, the objective of this study was to investigate adsorption kinetics, thermodynamics, and isotherms for the removal of morin and ARS on multiwalled carbon nanotubes (MWCNTs). The adsorption rates were evaluated with the pseudofirst-order, pseudosecond-order, and intraparticle diffusion model. The effects of temperature on the adsorption isotherms were determined, and the thermodynamic parameters of the changes of free energy (ΔG^0), enthalpy (ΔH^0), and entropy (ΔS^0) during adsorption at various temperatures were calculated.[33]

2. EXPERIMENTAL SECTION

2.1. Instruments and Reagents. ARS and morin (United States, Sigma-Aldrich) stock solution was prepared by dissolving the requires amount of their solid material in double-distilled water. The test solutions daily were prepared by diluting their stock solution to the desired concentrations. The concentration

Received: January 12, 2011
Accepted: March 28, 2011
Published: April 12, 2011

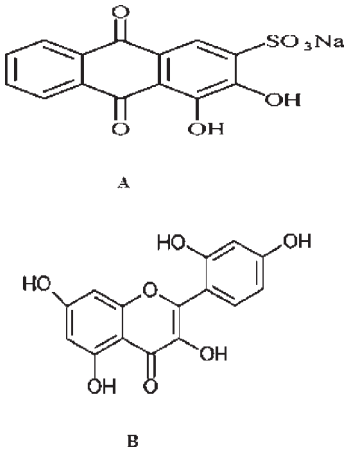

Figure 1. Structure of A: ARS; B: morin.

of morin and ARS was determined at (291, 259, and 423) nm, respectively. The pH measurements were done using a pH/ion meter model 682 (Metrohm, Switzerland), and absorption studies were carried out using a Jusco UV−visible spectrophotometer model V-570. All chemicals including KOH, HNO_3, and KCl MWCNTs with the highest purity available are purchased from Merck, Darmstadt, Germany.

2.2. Measurements of Dye Uptake. Concentrations of ARS and morin in solution were estimated quantitatively using the linear regression equations obtained by plotting its calibration curve over a range of concentrations. The dye adsorption capacities of adsorbent were determined at the time intervals in the range of (0 to 35) min and at various temperatures [(10 to 60) °C]. The equilibrium was established after 30 min for morin and ARS, respectively. The effect of initial pH on both dyes adsorptions was studied by at initial concentration of 100 mg·L^{-1} in the pH range of 1 to 5 by the addition of HCl or KOH. Dye adsorption experiments were also accomplished to obtain isotherms at various temperatures [(10 to 60) °C] and to a range of (50 to 200) mg·L^{-1} dye concentrations. The amount of dye adsorbed by adsorbent, q_e (mg·g^{-1}), was calculated by the following mass balance relationship:

$$q_e = (C_0 - C_e)V/W \quad (1)$$

where C_0 and C_e are the initial and equilibrium dye concentrations in solution, respectively (mg·L^{-1}), V the volume of the solution (L), and W is the mass (g) of the adsorbent used.

2.3. Structural Properties of CNTs. Carbon nanotubes form aggregated pores due to the entanglement of tens and hundreds of individual tubes that are adhered to each other as a result of van der Waals forces.[34−36] The dimensions of a mesopore or higher[37−45] are able to provide large external surface areas successible to large molecule contaminants. Hollow open-ended interiors of nanotubes (interstitial pore spaces between the tube bundles), boundary grooves of nanotube bundles, or the external surfaces of the CNTs are suitable sites for trapping and interaction with other species.[34,46] The interior space of CNTs is not suitable for adsorption due to its smaller size and close caps of CNTs. The interstitial spacing (formed between the bundles of nanotubes) is good with sites for the adsorption of a few low molecular weight small-sized adsorbates (e.g., metal ions).[36] The other two possibilities for potential adsorption sites provide large pore spaces that will be fully utilized by molecules of adsorbent; the accessible external surface area and presence of aggregated pores with volumes greater than the mesopore are considered biologically important[47] for adsorption.

3. RESULTS AND DISCUSSION

3.1. Absorption Effects. *3.1.1. Effect of pH.* Solution pH affects both aqueous chemistry and surface binding sites of the adsorbents. The effect of initial pH on the adsorption of ARS and morin was studied from pH of 1 to 5 at room temperature, at an initial dye concentration of 200 mg·L^{-1}, adsorbent dosage of 0.7 g·L^{-1} and 0.6 g·L^{-1} of the MWCNT, and contact time of 30 min at pH 1 for morin and ARS, respectively (see Figure 2). MWCNT experiments were performed using different initial solution pH values with no MWCNTs present. In these cases, the morin λ_{max} intensities in the UV−vis spectra were altered with pH. Therefore, the initial morin intensities were adjusted to the λ_{max} of each pH value. It was found that the adsorption capacity of both morin and ARS decreased with increasing pH over the pH range 1 to 5. When the pH of the solution was approximately 1.0, the MWCNTs would have more positively charged sites through increased MWCNT functional group protonation than at higher pH values. The area of the morin molecule with high negative potential, that is, at the 4-keto-3,5-dihydroxy group from an electrostatic potential map of morin, would thus be attracted by electrostatic forces. By increasing the pH the morin molecule star to deprotonated and at pH 5, morin would be about 49 % in the neutral nondissociated form (1) (pK_2 = 4.8) and thus 61 % monodissociated through deprotonation of the most acidic 3-hydroxy group, and this negatively charged form would also be strongly attracted to the MWCNT. This electrostatic attraction plays an important role in enhancing the dye uptake in silk fibers.[20]

The hydrolysis constant value of the most acidic group of the dye molecule is low. This functional group can be easily dissociated at higher pH, and thus, the ARS molecule has net negative charges and its removal decreased. Higher uptakes of dye obtained at lower pH values may be due to the electrostatic attractions between these charged dye cations and the negatively charged adsorbent surface. A lower adsorption at higher pH values may be due to the abundance of OH^- ions and because of ionic repulsion between the negatively charged surface and the anionic dye molecules. There are also no more exchangeable anions on the outer surface of the adsorbent at higher pH values, and consequently the adsorption decreases. At lower pH, more protons will be available, thereby increasing electrostatic attractions between ARS and positively charged adsorption sites and causing an increase in its adsorption.

3.1.2. Effect of Ionic Strength. The ionic strength of the solution is one of the factors that controls both electrostatic and nonelectrostatic interactions between the adsorbate and the adsorbent surface. We determined if the ongoing adsorption process was affected by salt (ionic strength). The dye adsorption would be affected not only by the pH value on the electron-donating capability and temperature on the change of entropy and heat of reaction, but also by the salt concentration on the hydrophobic and electrostatic interaction between dye and surface functional adsorptive sites of the adsorbent.

Dye adsorption studies over MWCNT were carried out at sodium chloride concentrations of (0 and 4) mol·L^{-1} with the initial dye concentration of 50 mg·L^{-1} for ARS and 15 mg·L^{-1} for morin, pH of 1, and 0.7 g·L^{-1} and 0.6 g·L^{-1} adsorbent

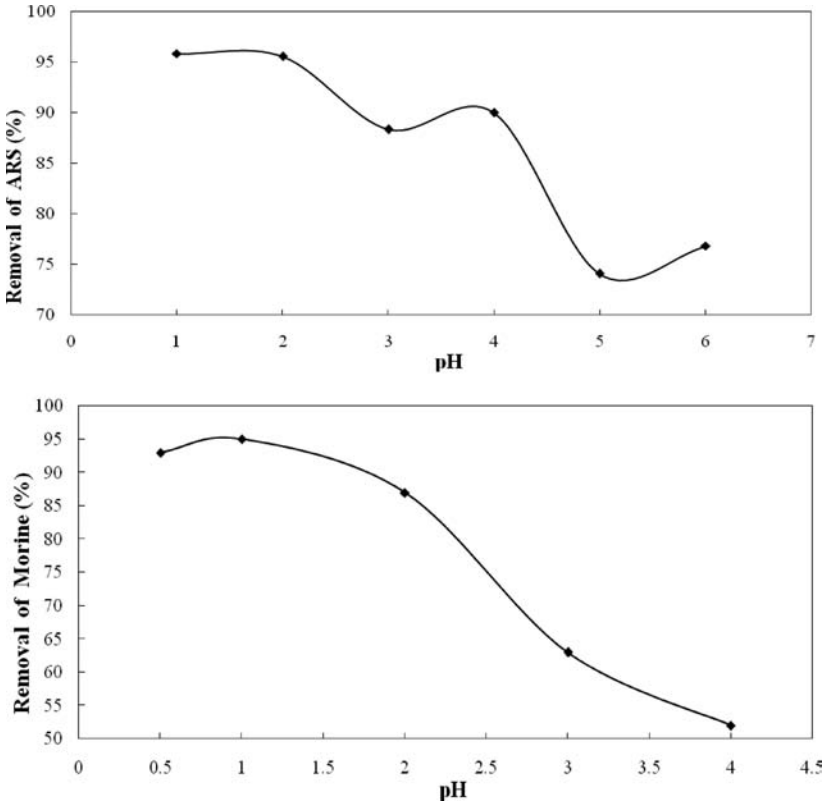

Figure 2. Effect of pH on adsorption of A: ARS; B: morin.

dosages for morin and ARS at a contact time of 30 min for both dyes. The adsorption capacities for the dyes were not significantly affected by increasing the KCl concentration from (0 to 4) $mol \cdot L^{-1}$. This indicates that Cl^- ions do not compete with functional groups of the dye molecules for MWCNT. The result of the proposed research indicates that the MWCNT can be used for removal of acidic dyes from salt containing water.

3.1.3. Effect of Adsorbent Dosage. The adsorption of dyes on MWCNT was studied by changing the quantity of adsorbent range of (0.2 to 0.7) $g \cdot L^{-1}$ and (0.2 to 0.8) $g \cdot L^{-1}$ for ARS and morin, respectively, with the dye concentration of 100 $mg \cdot L^{-1}$, room temperature, and pH of 1.0. It was seen that with increasing adsorbent dosage to (0.6 and 0.7) $g \cdot L^{-1}$ for ARS and morin the percent adsorption was increased. The increase in the adsorption with the increase in adsorbent dosage can be attributed to increased MWCNT surface area and the availability of more adsorption sites (see Figure 3). For the removal of both dyes the adsorption density of dyes decreased with the increase in adsorbent dosage.

3.1.4. Effect of Initial Dye Concentration. The initial concentration provides an important driving force to overcome all mass transfer resistance of all molecules between the aqueous and solid phases.[48−52] The effect of the initial concentration of morin and ARS in the range of (12.5 to 30) $mg \cdot L^{-1}$ and (45 to 100) $mg \cdot L^{-1}$ for morin and ARS, respectively. In the solutions, the rate of sorption onto MWCNT was studied at the pH of 1.0 at (0.6 and 0.7) $g \cdot L^{-1}$ of morin and ARS. Increasing the initial dye concentrations leads to an increase in the amount of adsorbed dye. These results suggest that the available sites on the adsorbent are the limiting factor for dye biosorption.[48]

By increasing the initial dye concentration the percentage of dye removal decreased, although the actual amount of dye adsorbed per unit mass of increased. This increase is due to the decrease in resistance to the uptake of solute from dye solution. The initial concentration provides an important driving force to overcome the mass transfer resistance of dye between the aqueous and the solid phases.

3.1.5. Effect of Contact Time on Dye Removal. The effects of contact time at room temperature on the sorption of both dyes are depicted in Figure 4. As can be seen from Figure 4 when the contact time was increased, the amount of adsorbed dye was not drastically increased. But for MWCNTs at the beginning the adsorption rate was fast as the dye ions were adsorbed by the exterior surface of the MWCNT. The percentage removal of dyes was greater at lower initial concentrations and was smaller at higher initial concentrations. In the dye adsorption process, initially dye molecules have to first encounter the boundary layer effect, and then they have to diffuse from boundary layer film onto the adsorbent surface and finally diffuse into the porous structure of the adsorbent. This phenomenon will take a relatively longer contact time. These results clearly indicate that the adsorption of dyes from its aqueous solution was dependent on its initial concentration. When the adsorption of the exterior surface reached saturation, the dye ions exerted onto the pores of the adsorbent particles and were adsorbed by the interior surface of the particle. This phenomenon takes a relatively long contact time.[53−59]

3.1.6. Effect of Temperature on Dye Removal. Various textile dye effluents are produced at relatively high temperatures; therefore, temperature can be an important factor for the real application of the MWCNT. To determine whether the ongoing adsorption process was endothermic or exothermic, respective studies over MWCNT were carried out at temperatures in the range of (283 to 333) K at (50 and 15) $mg \cdot L^{-1}$, pH 1, and a

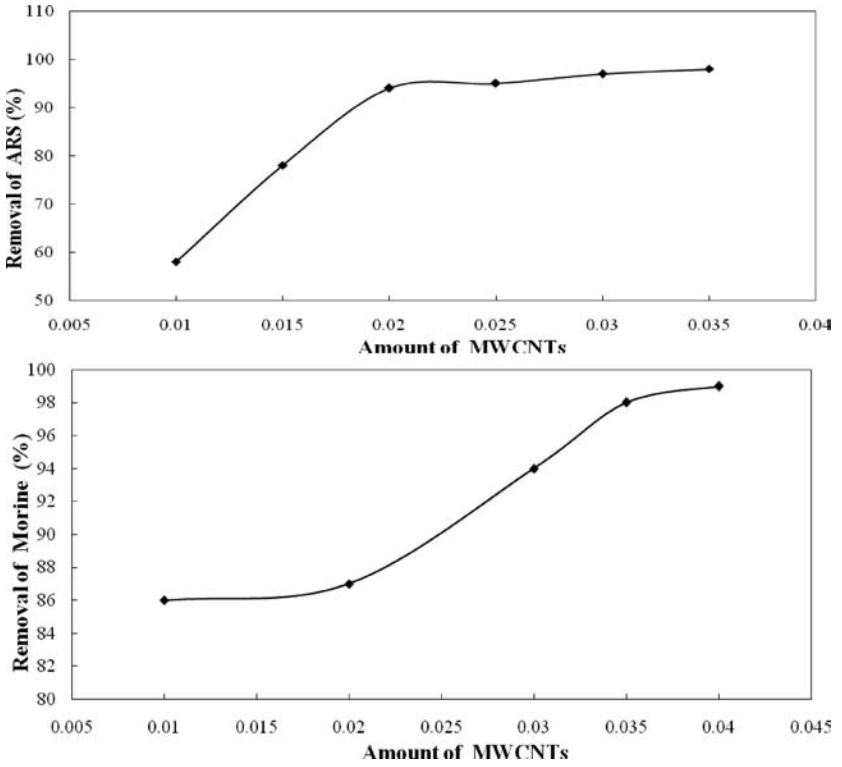

Figure 3. Effect of amount of MWCNTs for A: ARS; B: morin.

contact time of 30 min for ARS and morin, respectively. In general, the adsorption of both dyes increased with an increase in temperature, which indicates that the process was endothermic in both cases.

The adsorption of a solute from the solution phase onto the solid−liquid interface occurs by dislodging the solvent molecule (water) from the interfacial region. Probably with a rise in temperature from (283.15 to 303.15) K, the interaction between solvent and solid surface reduced exposing a greater number of adsorption sites as reported earlier. This enhanced the possibility of interaction between dye and adsorbents. In addition, at elevated temperatures, an increase in free volume occurred, which also favored adsorption.[60] As shown in Figure 4, the increase of equilibrium uptake with a further increase in temperature indicates that the dye sorption process is endothermic.

3.2. Kinetics Study. Adsorption kinetics is one of the most important characteristics which govern the solute uptake rate; it represents the adsorption efficiency of the adsorbent and, therefore, determines its potential applications. According to adsorption rates, the kinetics increased dramatically in the first 10 min and reached apparent equilibrium gradually within 30 min. Since MWCNTs do not have a porous-like structure, the adsorbate will likely move from the exterior surface to the inner surface of the pores on adsorbents to achieve equilibrium.[61,62]

To analyze the adsorption rate of both dyes onto CNTs, the Lagergren's first-order rate equation is employed:[63]

$$\ln(q_e - q_t)/q_e = -k_1 t \quad (2)$$

where q_t are the amounts of dye adsorbed onto CNTs at time t ($mg \cdot g^{-1}$) and k_1 is the first-order rate constant (min^{-1}). The k_1 values under various temperatures can be determined by the slope of a linear plot of $\ln[(q_e - q_t)/q^e]$ versus t and are given in Table 1. The correlation coefficients (R^2) are all > 0.96 indicating that the kinetics of dye adsorption by CNTs follows the first-order rate law. The k_1 value increased with a rise in temperature, which could be explained by the fact that the increasing temperature results in a rise in diffusion rate of dye molecules across the external boundary layer and within the pores of CNTs due to the result of decreasing solution viscosity. However, the temperature dependence of the k_1 value is inconsistent with the temperature dependence of the q_e value. This may be explained by the fact that the adsorption rate is faster than the desorption rate at a low temperature, but the desorption rate is more sensitive to temperature and becomes greater at a high temperature. Therefore, adsorption would dominate at lower temperatures, while desorption would dominate at higher temperatures.[64,65]

3.2.1. Pseudofirst-Order Equation. The adsorption kinetic data were described by the Lagergren pseudofirst-order model,[66] which is the earliest known equation describing the adsorption rate based on the adsorption capacity. The Lagergren equation is commonly expresses as follows:

$$dq_t/d_t = k_1(q_e - q_t) \quad (3)$$

where q_e and q_t are the adsorption capacity at equilibrium and at time t, respectively ($mg \cdot g^{-1}$) and k_1 is the rate constant of pseudofirst order adsorption ($L \cdot min^{-1}$). Integrating eq 3 for the boundary conditions $t = 0$ to $t = t$ and $q_t = 0$ to $q_t = q_t$ gives:

$$\log(q_e/q_e - q_t) = k_1/2.303t \quad (4)$$

Equation 4 can be rearranged to obtain the following linear form:

$$\log(q_e - q_t) = \log(q_e) - k_1/2.303t \quad (5)$$

The values of $\log(q_e - q_t)$ versus t can be plotted to give a linear relationship from which k_1 and q_e can be determined from its

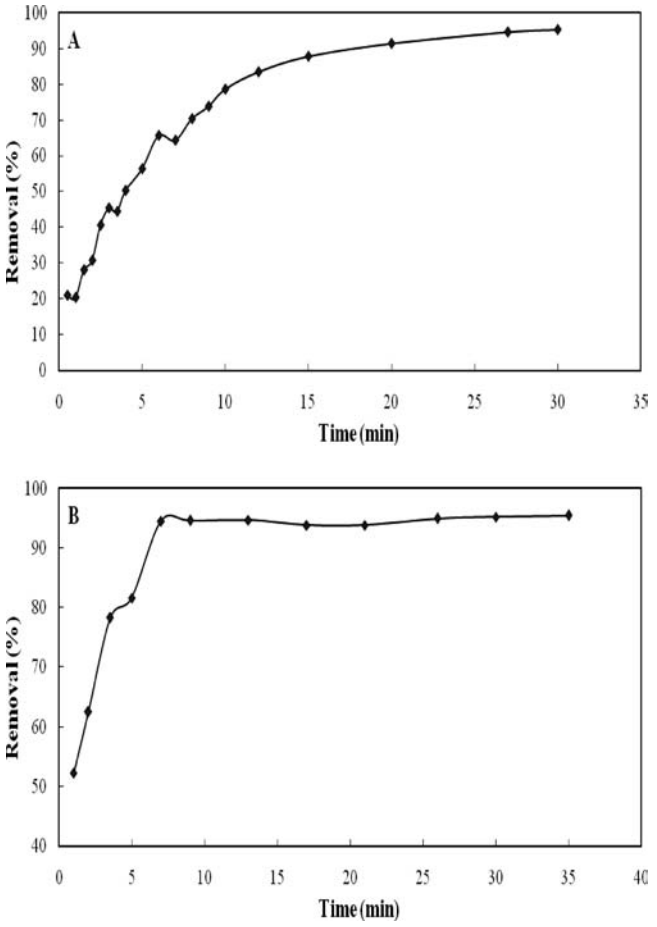

Figure 4. Effect of contact time on the removal of A:ARS, B: morin.

slope and intercept (Table 1). If the intercept dose not equal q_e then the reaction is not likely to be a first-order reaction even though this plot has a high correlation coefficient with the experimental data.[67] The variation in rate should be proportional to the first power of concentration for strict surface adsorption. However, the relationship between initial solute concentration and rate of adsorption will not be linear when pore diffusion limits the adsorption process. It can be seen that the model at initial stages obeyed the first order with rapid adsorption but cannot be applied for the entire adsorption process. This indicates that the adsorption of the dye is not a first-order reaction.

3.2.2. Pseudosecond-Order Equation. The adsorption kinetics may be described by the pseudosecond-order model,[68] which is generally given in linear form:

$$(t/qt) = 1/k_2 q_e^{\ 2} + 1/q_e(t) \quad (6)$$

and second-order rate constants (initial sorption rate) is calculated by the following eq 7:

$$h = k_2 q_e^{\ 2} \quad (7)$$

Given the nonapplicability of the first-order model for the entire adsorption process, the plots of t/q_t versus t give a straight line for all of the initial dye concentrations, confirming the applicability of the pseudosecond-order equation. Values of k_2 and equilibrium adsorption capacity q_e were calculated from the intercept and slope of the plots of t/q_t versus t, respectively. The

Table 1. Kinetic Parameters for the Adsorption of Dyes (A: ARS, B: Morin) onto the Adsorbent

		dye	
model		A	B
first-order kinetics	k_1	0.191	0.078
	q_e(calc)	99.311	4.503
	R^2	0.958	0.658
second-order kinetics	k_2	0.002	0.005
	q_e(calc)	111.111	21.505
	R^2	0.998	0.999
	h	26.316	23.309
intraparticle diffusion	K_{diff}	−0.247	5.418
	C	25.14	5.887
	R^2	0.982	0.983
Elovich	β	0.045	0.371
	R^2	0.986	0.837
q_e(exp)		166.66	21.171

values of R^2 and q_e also indicated that this equation produced better results (Table 1): at all concentrations and sorbent doses, R^2 values for pseudosecond-order kinetic model were found to be higher (between 0.991 and 0.996), and the calculated q_e values are mainly near to the experimental data. This indicates that ARS and morin on the MWCNT adsorption system obeys the pseudosecond-order kinetic model for the entire sorption period.

3.2.3. Intraparticle-Diffusion Model. In general, the dye sorption is governed by either the liquid phase mass transport rate or through the intraparticle mass transport rate. Pore-diffusion models should be formulated so as to consider not only the particle size but also the particle shape reported in the literature.[69,70]

The adsorption process is a diffusive mass transfer process where the rate can be expressed in terms of the square root of time (t). The intraparticle-diffusion model is expressed as follows:[71]

$$q_t = k_i t^{0.5} + I \quad (8)$$

where q_t is the fraction dye uptake ($mg \cdot g^{-1}$) at time t, k_i is the intraparticle-diffusion rate constant ($mg \cdot (g \cdot min^{0.5})^{-1}$), and I is the intercept ($mg \cdot g^{-1}$). The plot of q_t versus $t^{0.5}$ will give k_i as the slope and I as the intercept. The intercept I represents the effect of boundary layer thickness, and its minimum value shows that the process is less boundary-layer-controlled. The plot of q_t versus $t^{0.5}$ for the initial dye concentration of (50 and 15) $mg \cdot L^{-1}$ for ARS and morin is represented. Although the plots are nonlinear in nature, the data points can be better represented by double lines with a difference in slope (k_i) and intercept (I). The values of k and I are summarized in Table 1 along with the regression constant (R^2) for different temperatures. In the first straight line, the sudden increase (within a short time period) in slope signifies that the ARS and morin molecules are transported to the external surface of MWCNT particles through film diffusion, and its rate is very fast. After that, dye molecules enter into the solid phase particle by intraparticle diffusion through the pore which is represented in second straight line.[72]

3.3. Sorption Isotherms. *3.3.1. Equilibrium of Sorption.* The successful representation of the dynamic adsorptive separation of solute from solution onto an adsorbent depends upon a good

description of the equilibrium separation between the two phases. It is possible to depict the equilibrium adsorption isotherms by plotting solid phase concentration (q_{eq}; mg·g^{-1}) against liquid phase concentration (C_{eq}; mg·L^{-1}) of solute.[73] To discover the adsorption capacity of MWCNTs the experimental data were analyzed by the Langmuir, Freundlich, Tempkin, Dubinin and Radushkevich (D-R), and Harkins−Jura (H-J) isotherm equations. The isotherms of morin and ARS adsorption on MWCNT are of L-type, indicating that they have a high affinity for MWCNTs, and the constant parameters of the isotherm equations were calculated (Tables 2 and 3).

3.3.2. Langmuir Isotherm. The theoretical Langmuir sorption isotherm[74] is valid for the adsorption of a solute from a liquid solution as monolayer adsorption on a surface containing a finite number of identical sites. The model is based on several basic assumptions: (i) the sorption takes place at specific homogeneous sites within the adsorbent; (ii) once a dye molecule occupies a site; (iii) the adsorbent has a finite capacity for the adsorbate (at equilibrium); (iv) all sites are identical and energetically equivalent. The Langmuir isotherm model assumes uniform energies of adsorption onto the surface without transmigration of adsorbate in the plane of the surface. Therefore, the Langmuir isotherm model was chosen for the estimation of the maximum adsorption capacity corresponding to complete monolayer coverage on the sorbent surface. The nonlinear equation of Langmuir isotherm model can be written as follows:

$$q_e = Q_m K_a C_e/(1 + K_a C_e) \quad (9)$$

where C_e and q_e are the equilibrium liquid-phase concentrations of dyes and amount of dye adsorbed onto MWCNTs, respectively (mg·L^{-1} and mg·g^{-1}); Q_m is the maximum adsorption capacity reflected on a complete monolayer (mg·g^{-1}); K_a is the adsorption equilibrium constant (L·mg^{-1}) that is related to the apparent energy of sorption. The Langmuir isotherm parameters can be obtained from its linearized form (eq 10) and presented in Table 2:

$$C_e/q_e = 1/(K_a Q_m) + (1/Q_m)*C_e \quad (10)$$

A plot of C_e/q_e versus C_e should indicate a straight line of slope $1/Q_m$ and an intercept of $1/(K_a Q_m)$.

The results obtained from the four forms of the Langmuir model for the removal of dyes onto MWCNTs are shown in Table 2. The correlation coefficients reported in Table 3 showed strong positive evidence on the adsorption of dyes onto MWCNTs following the Langmuir and Tempkin isotherms. For Langmuir the experimental data obtained were found to be applicable only to the Langmuir-1 form depending on the high correlation coefficients $R^2 > 0.999$, while the other three linear forms of the Langmuir model represented the lower correlation coefficients. The fact that the Langmuir isotherm fits the experimental data very well may be due to the homogeneous distribution of active sites on the MWCNTs surface, since the Langmuir equation assumes that the surface is homogeneous.[75]

3.3.3. Freundlich Isotherm. The Freundlich isotherm model (Table 3) is valid for multilayer adsorption and is derived by

Table 2. Isotherm Parameters Obtained from Four Linear Forms of the Langmuir Model for the Adsorption of Dyes (A: ARS, B: Morin) onto the Adsorbent

model	parameters	dye	
		A	B
Langmuir-1: $C_e/q_e = (1/K_aQ_m) + C_e/Q_m$	Q_m (mg·g^{-1})	161.290	26.247
	K_a (L·mg^{-1})	0.681	6.568
	R^2	0.996	0.999
Langmuir-2: $1/q_e = 1/(K_aQ_mC_e) + 1/Q_m$	Q_m (mg·g^{-1})	149.253	25.510
	K_a (L·mg^{-1})	0.925	16.333
	R^2	0.901	0.966
Langmuir-3: $q_e = Q_m - q_e/(K_aC_e)$	Q_m (mg·g^{-1})	151.73	25.574
	K_a (L·mg^{-1})	1.012	15.051
	R^2	0.856	0.950
Langmuir-4: $q_e/C_e = K_aQ_m - K_aq_e$	Q_m (mg·g^{-1})	156.31	25.721
	K_a (L·mg^{-1})	0.866	15.248
	R^2	0.856	0.950

Table 3. Isotherm Constant Parameters and Correlation Coefficients Calculated for the Adsorption of Dyes (A: ARS, B: Morin) onto the Adsorbent

isotherm	parameters	dye	
		A	B
Langmuir-1: $1/q_e = 1/(K_aQ_mC_e) + 1/Q_m$	Q_m (mg·g^{-1})	161.290	26.247
	K_a (L·mg^{-1})	0.681	6.568
	R^2	0.996	0.999
Freundlich: $\ln q_e = \ln K_F + (1/n) \ln C_e$	$1/n$	0.197	0.061
	K_F (L·mg^{-1})	86.916	22.735
	R^2	0.938	0.993
Tempkin: $q_e = B_1 \ln K_T + B_1 \ln C_e$	B_1	22.12	1.483
	K_T (L·mg^{-1})	47.266	9719.98
	R^2	0.951	0.995
Dubinin and Radushkevich (D-R): $\ln q_e = \ln Q_s - B\varepsilon^2$	Q_s (mg·g^{-1})	144.619	25.239
	B	$5 \cdot 10^{-7}$	$1 \cdot 10^{-8}$
	E (kJ·mol^{-1}) = $1/(2B)^{1/2}$	1000.0	7071.067
	R^2	0.981	0.944
Harkins-Jura (H-J): $1/q_e^2 = (B_2/A) - (1/A) \log C_e$	A	16666.66	2000
	B_2	1.667	4
	R^2	0.81	0.986

dx.doi.org/10.1021/je2000414 |J. Chem. Eng. Data 2011, 56, 2511–2520

assuming a heterogeneous surface with interaction between adsorbed molecules with a nonuniform distribution of heat of sorption over the surface. The application of the Freundlich equation suggests that the sorption energy exponentially decreases on completion of the sorption centers of an adsorbent. It can be expressed in the linear form as follows.[60,76]

$$\ln q_e = \ln K_F + 1/n \ln C_e \quad (11)$$

where q_e is the equilibrium dye concentration on the adsorbent ($mg \cdot g^{-1}$), C_e the equilibrium dye concentration in solution ($mg \cdot L^{-1}$), and K_F ($mg \cdot g^{-1}$) and n are isotherm constants indicating the capacity and empirical parameter related to the intensity of the adsorption, respectively. The value of n varies with the heterogeneity of the adsorbent, and for favorable adsorption process the value of n should be less than 10 and higher than unity.[77,78]

The slope of plot $(1/n)$ in the range of 0 and 1 is a measure of adsorption intensity or surface heterogeneity, becoming more heterogeneous as its value gets closer to zero. The values of K_F and $1/n$ were determined from the intercept and slope of the linear plot of ln q_e versus ln C_e, respectively (Table 3).

3.3.4. Tempkin Isotherm. Tempkin and Pyzhev[79] considered the effect of some indirect sorbate/adsorbate interactions on the adsorption isotherm. This assumes that the heat of adsorption of all of the molecules in a layer decreases linearly with the surface coverage of adsorbent due to sorbate−adsorbate interactions. This adsorption is characterized by a uniform distribution of binding energies. The linear form of the Tempkin isotherm equation is represented by the following equation.[48]

$$q_e = B_1 \ln K_T + B_1 \ln C_e \quad (12)$$

where $B_1 = RT/b$, T is the absolute temperature in Kelvin, R the universal gas constant ($8.314\ J \cdot K^{-1} \cdot mol^{-1}$), K_T the equilibrium binding constant, and the constant B_1 is related to the heat of adsorption. Values of B_1 and K_T were calculated from the plot of q_e against ln C_e (Table 3).

3.3.5. Dubinin−Radushkevich (D-R) Isotherm. Another equation used in the analysis of isotherms was proposed by Dubinin−Radushkevich.[80] The D-R model was applied to estimate the porosity apparent free energy and the characteristics of adsorption,[81,82] The D-R isotherms does not assume a homogeneous surface or constant sorption potential, and it has commonly been applied in the following form (eq 18). Its linear form can be shown in eq 13:

$$q_e = Q_m \exp(-K\varepsilon^2) \quad (13)$$

$$\ln q_e = \ln Q_m - K\varepsilon^2 \quad (14)$$

where K is a constant related to the adsorption energy, Q_m the theoretical saturation capacity, ε is the Polanyi potential can be calculated from eq 15:

$$\varepsilon = RT \ln(1 + 1/C_e) \quad (15)$$

The slope of the plot of ln q_e versus ε^2 gives K ($mol^2 \cdot (kJ^2)^{-1}$), and the intercept yields the adsorption capacity, Q_m ($mg \cdot g^{-1}$). The mean free energy of adsorption (E), defined as the free energy change when one mole of ion is transferred from infinity in solution to the surface of the sorbent, was calculated from the K value using the following relation (eq 16):[83]

$$E = 1/(2K)^{1/2} \quad (16)$$

Calculated D-R constants for the adsorption of dyes on MWCNTs are shown in Table 3; the values of correlation coefficients are much lower than other isotherm values mentioned above. In this case, the D-R equation represents the poorer fit of experimental data than the other isotherm equation. Moreover, the maximum capacity Q_m obtained using the D-R isotherm model for the adsorption of dyes is 24.668 $mg \cdot g^{-1}$ on the MWCNT dose of 1 $g \cdot L^{-1}$, which is close to half of that obtained (40.650 $mg \cdot g^{-1}$) from the Langmuir-1 isotherm model (Table 3).

3.3.6. Harkins−Jura Adsorption Isotherm. The Harkins−Jura adsorption isotherm[84] can be expressed as:

$$1/q_e^2 = (B^2/A) - (1/A)\log C_e \quad (17)$$

where B_2 and A are the isotherm constants. The Harkins−Jura adsorption isotherm accounts to multilayer adsorption and can be explained with the existence of a heterogeneous pore distribution. $1/q_e^2$ was plotted versus log C_e. Isotherm constants and correlation coefficients are summarized in Table 3. The Tempkin models fit the adsorption of dyes on MWCNT adsorbent best, respectively.

3.4. Thermodynamics Study. The adsorption on solids is classified into physical adsorption and chemical adsorption, but the dividing line between the two is not sharp. However, physical adsorption is nonspecific, and the variation of energy for physical adsorption is usually substantially smaller than that of chemical adsorption. Chemical adsorption is similar to ordinary chemical reactions in that it is highly specific. Typically, ΔH for physical adsorption ranges from (−4 to −40) $kJ \cdot mol^{-1}$, compared to that of chemical adsorption ranging from (−40 to −800) $kJ \cdot mol^{-1}$. As shown in Table 4, the ΔH values suggest that the adsorption process might be considered as physical adsorption in nature.

In general, in the external mass transport process, the values of the diffusion coefficient increase as the temperature of adsorption increases. Increasing the temperature leads to a decrease in the thickness of the boundary layer surrounding the adsorbent and the mass transport resistance of the adsorbate in the boundary layer. Thus, the diffusion rate of dyes in the external mass transport process increases with temperature, while in intraparticle diffusion the coefficient of diffusion values decreases with increasing temperature. At low temperature, the diffusion coefficient of external mass transport is slightly lower than the diffusion coefficient of intraparticle diffusion. So, at low temperature, dye adsorption is limited by the external mass transport. With the increase of temperature external mass transport begins to play a major role in dye adsorption by chitosan. One of the reasons for the positive changes of the enthalpy and entropy could be the release of numerous water molecules.

The thermodynamic parameters, free energy change ($\Delta G°$), enthalpy change ($\Delta H°$), and entropy change ($\Delta S°$) for the adsorption of dye onto CNTs were calculated using the following equations (Table 4):[83]

$$\Delta G° = -RT \ln K_0 \quad (18)$$

$$\Delta S° = \Delta H° - \Delta G°T \quad (19)$$

where K_0 is the thermodynamic equilibrium constant. As the dye concentration in the solution decreases and approaches 0, values of K_0 are obtained by plotting a straight line of (q_e/C_e) versus q_e

Table 4. Thermodynamics Parameters for the Adsorption of Dyes (A: ARS, B: Morin) onto the Adsorbent

parameter	C_0 mg·L^{-1}		temperature, K 283.15	293.15	303.15	313.15	323.15	333.15
k_c	dye	B	0.608	1.327	1.509		2.287	
		A	2.182	3.737	3.959	6.041	11.65	37.893
ΔG^0 (J·mol^{-1})		B	1169.572	−689.742	−1037.68		−2223.14	
		A	−1837.24	−3213.2	−3467.87	−0.4682.81	−6597.43	−10067.7

parameters	dye A	dye B
ΔS^0 (J·mol^{-1}·K^{-1})	39.99	23.192
ΔH^0 (kJ·mol^{-1})	145.911	79.453
E_a (kJ·mol^{-1})	34.844	12.704
S^*	$2.400 \cdot 10^{-6}$	$7.720 \cdot 10^{-5}$

based on a least-squares analysis and extrapolating q_e to 0. The intercept of the vertical axis gives the K_0 value. The $\Delta H°$ is determined from the slope of the regression line after plotting ln K_0 against the reciprocal of absolute temperature, $1/T$. The $\Delta G°$ and $\Delta S°$ are determined from eqs 18 and 19, respectively. Table 4 summarizes the values of these thermodynamic parameters. Negative $\Delta H°$ indicates the exothermic nature of adsorption process. This is supported by the decrease of dye adsorption onto CNTs with a rise in temperature. Negative $\Delta G°$ suggests that the adsorption process is spontaneous with a high preference of dye molecules for the CNTs. Positive $\Delta S°$, which reflects the affinity of the CNTs for the dye and the increase of randomness at the solid/liquid interface during adsorption process, may be due to the release of water molecules produced by molecule exchange between dye molecules and the functional groups attached on the CNT surface.

First, all of the samples present a negative standard free energy change and a positive standard entropy change, which indicates that the adsorption reactions are in general a spontaneous process and thermodynamically favorable. The positive standard entropy changes indicate that the degree of freedom increases at the solid−liquid interface during the adsorption of dye on MWCNTs. The dye in solution is surrounded by a tightly bound hydration layer where water molecules are more highly ordered than in the bulk water. When a molecule of dye comes into close interaction with the hydration surface of MWCNTs, the ordered water molecules in these two hydration layers are compelled and disturbed, thus increasing the entropy of water molecules.

Negative $\Delta G°$ suggests that the adsorption process is spontaneous with a high preference of dye molecules for the CNTs. Positive $\Delta S°$, which reflects the affinity of the CNTs for the dye and the increase of randomness at the solid−liquid interface during adsorption process, may be due to the release of water molecules produced by molecule exchange between dye molecules and the functional groups attached on the CNT surface.

AUTHOR INFORMATION

Corresponding Author

*Tel. and fax: (0098)-741-2223048. E-mail: m_ghaedi@mail.yu.ac.ir.

REFERENCES

(1) de Lima, R. O. A.; Bazo, A. P.; Salvadori, D. M. F.; Rech, C. M.; Oliveira, D. P.; Umbuzeiro, G. A. Mutagenic and carcinogenic potential of a textile azo dye processing plant effluent that impacts a drinking water source. *Mutat. Res.* **2007**, *626*, 53–60.

(2) Tsuboy, M. S.; Angeli, J. P. F.; Mantovani, M. S.; Knasmüller, S.; Umbuzeiro, G. A.; Ribeiro, L. R. Genotoxic, mutagenic and cytotoxic effects of the commercial dye CI Disperse Blue 291 in the human hepatic cell line HepG2. *Toxicol. in Vitro* **2007**, *21*, 1650–1655.

(3) Caritá, R.; Marin-Morales, M. A. Induction of chromosome aberrations in the Allium cepa test system caused by the exposure of seeds to industrial effluents contaminated with azo dyes. *Chemosphere* **2008**, *5*, 722–725.

(4) Pavan, F. A.; Dias, S. L. P.; Lima, E. C.; Benvenutti, E. V. Removal of congo red from aqueous solution by anilinepropylsilica xerogel. *Dyes Pigm.* **2008**, *76*, 64–69.

(5) Pavan, F. A.; Gushikem, Y.; Mazzocato, A. S.; Dias, S. L. P.; Lima, E. C. Statistical design of experiments as a tool for optimizing the batch conditions to methylene blue biosorption on yellow passion fruit and mandarin peels. *Dyes Pigm.* **2007**, *72*, 256–266.

(6) Pavan, F. A.; Lima, E. C.; Dias, S. L. P.; Mazzocato, A. C. Methylene blue biosorption from aqueous solutions by yellow passion fruit waste. *J. Hazard. Mater.* **2008**, *150* (3), 703–71.

(7) Iqbal, M. J.; Ashiq, M. N. Adsorption of dyes from aqueous solutions on activated charcoal. *J. Hazard. Mater.* **2007**, *B139*, 57–66.

(8) Wu, Z.; Joo, H.; Ahna, I.-S.; Haama, S.; Kima, J.-H.; Lee, K. Organic dye adsorption on mesoporous hybrid gels. *Chem. Eng. J.* **2004**, *102*, 277–282.

(9) Septhum, C.; Rattanaphani, S.; Bremner1, J. B.; Rattanaphani, V. An Adsorption Study of Alum-morin Dyeing onto Silk Yarn. *Fibers Polym.* **2009**, *10*, 481–487.

(10) Zheng, F.; Baldwin, D. L.; Fifield, L. S.; Anheier, N. C.; Aardahl, C. L.; Grate, J. W. Single-walled carbon nanotube paper as a sorbent for organic vapor preconcentration. *Anal. Chem.* **2006**, *78*, 2442–2446.

(11) Zhou, Q. X.; Wang, W. D.; Xiao, J. P. Preconcentration and determination of nicosulfuron, thifensulfuron-methyl and metsulfuron-methyl in water samples using carbon nanotubes packed cartridge in combination with high performance liquid chromatography. *Anal. Chim. Acta* **2006**, *559*, 200–206.

(12) Zhou, Q. X.; Xiao, J. P.; Wang, W. D.; Liu, G. G.; Shi, Q. Z.; Wang, J. H. Determination of atrazine and simazine in environmental water samples using multiwalled carbon nanotubes as the adsorbents for preconcentration prior to high performance liquid chromatography with diode array detector. *Talanta* **2006**, *68*, 1309–1315.

(13) Liang, P.; Ding, Q.; Song, F. Application of multiwalled carbon nanotubes as solid phase extraction sorbent for preconcentration of trace copper in water samples. *J. Sep. Sci.* **2005**, *28*, 2339–2343.

(14) Tuzen, M.; Saygi, K. O.; Soylak, M. Solid phase extraction of heavy metal ions in environmental samples on multiwalled carbon nanotubes. *J. Hazard. Mater.* **2008**, *152*, 632–639.

(15) Smart, S. K.; Cassady, A. I.; Lu, G. Q.; Martin, D. J. The biocompatibility of carbon nanotubes. *Carbon* **2006**, *44*, 1034–1047.
(16) Lu, C.; Chung, Y.-L.; Chang, K.-F. Adsorption thermodynamic and kinetic studies of trihalomethanes on multiwalled carbon nanotubes. *J. Hazard. Mater.* **2006**, *B138*, 304–310.
(17) Mauter, M. S.; Elimelech, M. Environmental applications of carbon-based nanomaterials. *Environ. Sci. Technol.* **2008**, *42*, 5843–5859.
(18) Fugetsu, B.; Satoh, S.; Shiba, T.; Mizutani, T.; Lin, Y.; Terui, N.; Nodasaka, Y.; Sasa, K.; Shimizu, K.; Akasaka, T. Caged multiwalled carbon nanotubes as the adsorbents for affinity-based elimination of ionic dyes. *Environ. Sci. Technol.* **2004**, *38*, 6890–6896.
(19) Yang, K.; Zhu, L.; Xing, B. Adsorption of polycyclic aromatic hydrocarbons by carbon nanomaterials. *Environ. Sci. Technol.* **2006**, *40*, 1855–1861.
(20) Chin, C. J. M.; Shih, L. C.; Tsai, H. J.; Liu, T. K. Adsorption of o-xylene and p-xylene from water by SWCNTs. *Carbon* **2007**, *45*, 1254–1260.
(21) Sheng, G. D.; Shao, D. D.; Ren, X. M.; Wang, X. Q.; Li, J. X.; Chen, Y. X.; Wang, X. K. Kinetics and thermodynamics of adsorption of ionizable aromatic compounds from aqueous solutions by as-prepared and oxidized multiwalled carbon nanotubes. *J. Hazard. Mater.* **2010**, *178*, 505–516.
(22) Long, R. Q.; Yang, R. T.; Am, J. Carbon nanotubes as superior sorbent for dioxin removal. *Chem. Soc.* **2001**, *123*, 2058–2059.
(23) Peng, X.; Li, Y.; Luan, Z.; Di, Z.; Wang, H.; Tian, B.; Jia, Z. Adsorption of 1,2-dichlorobenzene from water to carbon nanotubes. *Chem. Phys. Lett.* **2003**, *376*, 154–158.
(24) Lu, C.; Chung, Y. L.; Chang, K. F. Adsorption of trihalomethanes from water with carbon nanotubes. *Water Res.* **2005**, *39*, 1183–1189.
(25) Yang, K.; Zhu, L.; Xing, B. Adsorption of polycyclic aromatic hydrocarbons by carbon nanomaterials. *Environ. Sci. Technol.* **2006**, *40*, 1855–1861.
(26) Chin, C. J. M.; Shih, L. C.; Tsai, H. J.; Liu, T. K. Adsorption of o-xylene and p-xylene from water by SWCNTs. *Carbon* **2007**, *45*, 1254–1260.
(27) Liao, Q.; Sun, J.; Gao, L. Adsorption of chlorophenols by multi-walled carbon nanotubes treated with HNO_3 and NH_3. *Carbon* **2008**, *46*, 553–555.
(28) Chen, W.; Duan, L.; Zhu, D. Adsorption of polar and nonpolar organic chemicals to carbon nanotubes. *Environ. Sci. Technol.* **2007**, *41*, 8295–8300.
(29) Cho, H. H.; Smith, B. A.; Wnuk, J. D.; Fairbrother, D. H.; Ball, W. P. Influence of surface oxides on the adsorption of naphthalene onto multiwalled carbon nanotubes. *Environ. Sci. Technol.* **2008**, *42*, 2899–2905.
(30) Duran, A.; Tuzen, M.; Soylak, M. Preconcentration of some trace elements via using multiwalled carbon nanotubes as solid phase extraction adsorbent. *J. Hazard. Mater.* **2009**, *169*, 466–471.
(31) Tuzen, M.; Saygi, K. O.; Usta, C.; Soylak, M. Pseudomonas aeruginosa immobilized multiwalled carbon nanotubes as biosorbent for heavy metal ions. *Bioresour. Technol.* **2008**, *99*, 1563–1570.
(32) Tuzen, M.; Soylak, M. Multiwalled carbon nanotubes for speciation of chromium in environmental samples. *J. Hazard. Mater.* **2007**, *147*, 219–225.
(33) Chen, G.-C.; Shan, X.-Q.; Zhou, Y.-Q.; Shen, X.-e.; Huang, H.-L.; Khan, S. U. Adsorption kinetics, isotherms and thermodynamics of atrazine on surface oxidized multiwalled carbon nanotubes. *J. Hazard. Mater.* **2009**, *169*, 912–918.
(34) Agnihotri, S.; Mota, J. P. B.; Rostam-Abadi, M.; Rood, M. J. Structural characterization of single walled carbon nanotube bundles by experiment and molecular simulation. *Langmuir* **2005**, *21*, 896–904.
(35) Donaldson, K.; Aitken, R.; Tran, L.; Stone, V.; Duffin, R.; Forrest, G. Carbon nanotubes: a review of their properties in relation to pulmonary toxicology and workplace safety. *Toxicol. Sci.* **2006**, *92*, 5–22.
(36) Yan, X. M.; Shi, B. Y.; Lu, J. J.; Feng, C. H.; Wang, D. S.; Tang, H. X. Adsorption and desorption of atrazine on carbon nanotubes. *J. Colloid Interface Sci.* **2008**, *32*, 30–38.
(37) Benny, T. H.; Bandosz, T. J.; Wong, S. S. Effect of ozonolysis on the pore structure, surface chemistry, and bundling of single walled carbon nanotubes. *J. Colloid Interface Sci.* **2008**, *317*, 375–382.
(38) Chen, Y.; Liu, C.; Li, F.; Cheng, H. M. Pore structures of multi walled carbon nanotubes activated by air, CO_2 and KOH. *J. Porous Mater.* **2006**, *13*, 141–6.
(39) Lee, S. M.; Lee, S. C.; Jung, J. H.; Kim, H. J. Pore characterization of multi walled carbon nanotubes modified by KOH. *Chem. Phys. Lett.* **2005**, *416*, 251–255.
(40) Li, Y. H.; Wang, S.; Zhang, X.; Wei, J.; Xu, C.; Luan, Z. Adsorption of fluoride from water by aligned carbon nanotubes. *Mater. Res. Bull.* **2003**, *38*, 469–476.
(41) Liao, Q.; Sun, J.; Gao, L. Adsorption of chlorophenols by multi walled carbon nanotubes treated with HNO_3 and NH_3. *Carbon* **2008**, *46*, 544–561.
(42) Liu, Y.; Shen, Z.; Yokogawa, K. Investigation of preparation and structures of activated carbon nanotubes. *Mater. Res. Bull.* **2006**, *41*, 1503–1512.
(43) Mauter, S. M.; Elimelech, M. Environmental applications of carbon based nanomaterials. *Environ. Sci. Technol.* **2008**, *42*, 5843–5859.
(44) Niu, J. J.; Wang, J. N.; Jiang, Y.; Su, L. F.; Ma, J. An approach to carbon nanotubes with high surface area and large pore volume. *Microporous Mesoporous Mater.* **2007**, *100*, 1–5.
(45) Yang, K.; Zhu, L.; Xing, B. Adsorption of polycyclic aromatic hydrocarbons by carbon nanomaterials. *Environ. Sci. Technol.* **2006**, *40*, 1855–1861.
(46) Kang, S.; Herzberg, M.; Rodrigues, D. F.; Elimelech, M. Antibacterial effects of carbon nanotubes: size does matter. *Langmuir* **2008**, *a24*, 6409–6413.
(47) Upadhyayula, V. K. K.; Deng, S.; Mitchell, M. C.; Smith, G. B. Application of carbon nanotube technology for removal of contaminants in drinking water: A review. *Sci. Total Environ.* **2009**, *408*, 1–13.
(48) Colak, F.; Atar, N.; Olgun, A. Biosorption, of acidic dyes from aqueous solution by Paenibacillus macerans: Kinetic, thermodynamic and equilibrium studies. *Chem. Eng. J.* **2009**, *150*, 122–130.
(49) Shukla, A.; Zhang, Y.; Dubey, P.; Margrave, J. L.; Shukla, S. S. The role of sawdust in the removal of unwanted materials from water. *J. Hazard. Mater.* **2002**, *B95*, 137–152.
(50) Donmez, G.; Aksu, Z. Removal of chromium (VI) from saline wastewaters by Dunaliella species. *Process Biochem.* **2002**, *38*, 751–762.
(51) Kannan, N.; Susndaram, M. M. Kinetics and mechanism of removal of methylene blue by adsorption on various carbons-a comparative study. *Dyes Pigm.* **2001**, *51*, 25–40.
(52) Mall, I. D.; Srivastava, V. C.; Agarwal, N. K.; Mishra, I. M. Removal of congo red from aqueous solution by bagasse fly ash and activated carbon: kinetic study and equilibrium isotherm analyses. *Chemosphere* **2005**, *61*, 492–501.
(53) Jumasiah, A.; Chuah, T. G.; Gimbon, J.; Choong, T. S. Y.; Azni, I. Adsorption of basic dye onto palm kernel shell activated carbon: sorption equilibrium and kinetics studies. *Desalination* **2005**, *186*, 57–64.
(54) (a) Amin, N. K. Removal of reactive dye from aqueous solutions by adsorption onto activated carbons prepared from sugarcane bagasse pith. *Desalination* **2008**, *223*, 152–161. (b) Mittal, A.; Kaur, D.; Mittal, J. Batch and bulk removal of a triarylmethane dye, Fast Green FCF, from wastewater by adsorption over waste materials. *J. Hazard. Mater.* **2009**, *163*, 568–577.
(55) (a) Basar, C. A. Applicability of the various adsorption models of three dyes adsorption onto activated carbon prepared waste apricot. *J. Hazard. Mater.* **2006**, *B135*, 232–241. (b) Malik, P. K. Use of activated carbons prepared from sawdust and rice-husk for adsorption of acid dyes: a case study of acid yellow 36. *Dyes Pigm.* **2003**, *56*, 239–249.
(56) Chatterjee, S.; Chatterjee, S.; Chatterjee, B. P.; Guha, A. K. Adsorptive removal of congo red, a carcinogenic textile dye by chitosan hydrobeads: Binding mechanism, equilibrium and kinetics. *Colloids Surf., A* **2007**, *299*, 146–152.
(57) Rengaraj, S.; Kim, Y.; Joo, C. K.; Yi, J. Removal of copper from aqueous solutions by aminated and protonated mesoporous aluminas: kinetics and equilibrium. *J. Colloid Interface Sci.* **2004**, *273*, 14–21.

(58) Lagergren, S. Zur theorie der sogenannten adsorption geloster stoffe. *K. Sven. Vetenskapsakad. Handl.* **1898**, *24*, 1–39.
(59) Chien, S. H.; Clayton, W. R. Application of Elovich equation to the kinetics of phosphate release and sorption on soils. *Soil Sci. Soc. Am. J.* **1980**, *44*, 265–268.
(60) Crini, G.; Peindy, H. N.; Gimbert, F.; Robert, C. Removal of C. I. Basic Green 4 (Malachite Green) from aqueous solutions by adsorption using cyclodextrin based adsorbent: kinetic and equilibrium studies. *Sep. Purif. Technol.* **2007**, *53*, 97–110.
(61) Peng, X.; Li, Y.; Luan, Z.; Di, Z.; Wang, H.; Tian, B.; Jia, Z. Adsorption of 1,2-dichlorobenzene from water to carbon nanotubes. *Chem. Phys. Lett.* **2003**, *376*, 154–158.
(62) Chen, G.-C.; Shan, X.-Q.; Zhou, Y.-Q.; Shen, X.-e.; Huang, H.-L.; Khan, S. U. Adsorption kinetics, isotherms and thermodynamics of atrazine on surface oxidized multiwalled carbon nanotubes. *J. Hazard. Mater.* **2009**, *169*, 912–918.
(63) Tütem, E.; Apak, R.; Ünal, Ç. F. Adsorptive removal of chlorophenols from water by bituminous shale. *Water Res.* **1998**, *32*, 2315–2324.
(64) Thomson, W. J. *Introduction to Transport Phenomena*; Prentice Hall PTR: Upper Saddle River, NJ, 2000.
(65) Lu, C.; Chung, Y.-L.; Chang, K.-F. Adsorption thermodynamic and kinetic studies of trihalomethanes on multiwalled carbon nanotubes. *J. Hazard. Mater.* **2006**, *B138*, 304–310.
(66) Iqbal, M. J.; Ashiq, M. N. Adsorption of dyes from aqueous solutions on activated charcoal. *J. Hazard. Mater.* **2007**, *B139*, 57–66.
(67) Ho, Y. S.; McKay, G.; Wase, D. A. J.; Foster, C. F. Study of the sorption of divalentmetal ions on to peat. *Adsorpt. Sci. Technol.* **2000**, *18*, 639–650.
(68) Mittal, A.; Kaur, D.; Mittal, J. Applicability of waste materials—bottom ash and deoiled soya—as adsorbents for the removal and recovery of a hazardous dye, brilliant green. *J. Colloid Interface Sci.* **2008**, *326*, 8–17.
(69) Ruthven, D. M.; Loughlin, K. F. The effect of crystallite shape and size distribution on diffusion measurements in molecular sieves. *Chem. Eng. Sci.* **1971**, *26*, 577–584.
(70) Pignatello, J. J.; Ferrandino, F. J.; Huangm, L. Q. Elution of aged and freshly added herbicides from a soil. *Environ. Sci. Technol.* **1993**, *27*, 1563–1571.
(71) Weber, W. J.; Morriss, J. C. Kinetics of adsorption on carbon from solution. *J. Sanit. Eng., Div. Am. Soc. Civil Eng.* **1963**, *89*, 31–60.
(72) Mall, I. D.; Srivastava, V. C.; Agarwal, N. K.; Mishra, I. M. Adsorptive removal of malachite green dye from aqueous solution by bagasse fly ash and activated carbon-kinetic study and equilibrium isotherm analyses. *Colloids Surf., A.* **2005**, *264*, 17–28.
(73) Allen, S. J.; Gan, Q.; Matthews, R.; Jhonson, P. A. Comparison of optimized isotherm models for basic dye adsorption by kudzu. *Bioresour. Technol.* **2003**, *88*, 143–152.
(74) Langmuir, I. The constitution and fundamental properties of solids and liquids. *J. Am. Chem. Soc.* **1916**, *38*, 2221–2295.
(75) Abdelwahab, O. Evaluation of the use of loofa activated carbons as potential adsorbents for aqueous solutions containing dye. *Desalination* **2008**, *222*, 357–367.
(76) Waranusantigul, P.; Pokethitiyook, P.; Kruatrachue, M.; Upatham, E. S. Kinetics of basic dye (methylene blue) biosorption by giant duckweed (*Spirrodella polyrrhiza*). *Environ. Pollut.* **2003**, *125*, 385–392.
(77) Freundlich, H. M. F. Über die adsorption in lösungen. *Z. Phys. Chem. (Leipzig)* **1906**, *57A*, 385–470.
(78) Senturk, H. B.; Ozdes, D.; Gundogdu, A.; Duran, C.; Soylak, M. Removal of phenol from aqueous solutions by adsorption onto organomodified Tirebolu bentonite: Equilibrium, kinetic and thermodynamic study. *J. Hazard. Mater.* **2009**, *172*, 353–362.
(79) Tempkin, M. J.; Pyzhev, V. Kinetics of ammonia synthesis on promoted iron catalysis. *Acta Physiochim. URSS* **1940**, *12*, 327–356.
(80) Pearce, C. I.; Lioyd, J. R.; Guthrie, J. T. The removal of color from textile wastewater using whole bacterial cells: a review. *Dyes Pigm.* **2003**, *58*, 179–196.
(81) Dubinin, M. M. Modern state of the theory of volume filling of micropore adsorbents during adsorption of gases and steams on carbon adsorbents. *Zh. Fiz. Khim.* **1965**, *39*, 1305–1317.
(82) Radushkevich, L. V. Potential theory of sorption and structure of carbons. *Zh. Fiz. Khim.* **1949**, *23*, 1410–1420.
(83) Panda1, G. C.; Das1, S. K.; Guha, A. K. Jute stick powder as a potential biomass for the removal of congo red and rhodamine B from their aqueous solution. *J. Hazard. Mater.* **2009**, *164*, 374–379.
(84) Xue, Y.; Hou, H.; Zhu, S. Adsorption removal of reactive dyes from aqueous solution by modified basic oxygen furnace slag: Isotherm and kinetic study. *Chem. Eng. J.* **2009**, *147*, 272–279.